SANDIA REPORT

SAND2000-8437
Unlimited Release
Printed December 1999

Electroosmotic Fluid Motion and Late-Time Solute Transport at Non-Negligible Zeta Potentials

S. K. Griffiths, R. H. Nilson

Prepared by
Sandia National Laboratories
Albuquerque, New Mexico 87185 and Livermore, California 94550

Sandia is a multiprogram laboratory operated by Sandia Corporation, a Lockheed Martin Company, for the United States Department of Energy under Contract DE-AC04-94AL85000.

Sandia National Laboratories

Issued by Sandia National Laboratories, operated for the United States Department of Energy by Sandia Corporation.

Available to DOE and DOE contractors from
Office of Scientific and Technical Information
P.O. Box 62
Oak Ridge, TN 37831

Prices available from (703) 605-6000
Web site: http://www.ntis.gov/ordering.htm

Available to the public from
National Technical Information Service
U.S. Department of Commerce
5285 Port Royal Rd
Springfield, VA 22161

NTIS price codes
Printed copy: A03
Microfiche copy: A01

DISCLAIMER

Portions of this document may be illegible in electronic image products. Images are produced from the best available original document.

SAND2000-8437
Unlimited Release
Printed December 1999

Electroosmotic Fluid Motion and Late-Time Solute Transport at Non-Negligible Zeta Potentials

Stewart K. Griffiths and Robert H. Nilson
Sandia National Laboratories
Livermore, California 94551-0969

ABSTRACT

Analytical and numerical methods are employed to determine the electric potential, fluid velocity and late-time solute distribution for electroosmotic flow in a tube and channel when the zeta potential is not small. The electric potential and fluid velocity are in general obtained by numerical means. In addition, new analytical solutions are presented for the velocity in a tube and channel in the extremes of large and small Debye layer thickness. The electroosmotic fluid velocity is used to analyze late-time transport of a neutral non-reacting solute. Zeroth and first-order solutions describing axial variation of the solute concentration are determined analytically. The resulting expressions contain eigenvalues representing the dispersion and skewness of the axial concentration profiles. These eigenvalues and the functions describing transverse variation of the concentration field are determined numerically using a shooting technique. Results are presented for both tube and channel geometries over a wide range of the normalized Debye layer thickness and zeta potential. Simple analytical approximations to the eigenvalues are also provided for the limiting cases of large and small values of the Debye layer thickness. The methodology developed here for electroosmotic flow is also applied to the Taylor problem of late-time transport and dispersion in pressure-driven flows.

INTRODUCTION

Microchannel devices are finding increased use in the identification and synthesis of chemical and biological species. Employing transverse channel dimensions from a few microns to about one millimeter, such systems may permit the miniaturization and large-scale integration of many chemical processes in a manner analogous to that already achieved in microelectronics. Applications for microchannel devices now under development include such diverse processes as DNA sequencing, immunoassay, the identification of explosives, identification of chemical and biological warfare agents, and the synthesis of chemicals and drugs.

Electroosmotic flows [1,2] offer two important benefits over pressure-driven flows for solute transport in microchannel devices. First, fluid speeds in electroosmotic flows are independent of the transverse dimension of the tube or channel over a wide range of conditions, making this technique for driving fluid motion extensible to extremely small physical scales. In contrast, pressure-driven flows require a pressure gradient that increases inversely with the square of the minimum transverse dimension to maintain a given fluid speed. Second, the profile of the electroosmotic fluid velocity across a tube or channel is essentially flat, again over a wide range of conditions. All transverse variation in the axial speed is confined to a small region adjacent to the tube or channel walls and comparable in thickness to the electric Debye layer. The benefit of this flat velocity profile is that solute samples may be transported over long ranges with very little dispersion due to nonuniform fluid speeds.

In a previous study [3], we employed analytical methods to investigate the late-time transport of a neutral non-reacting solute in an incompressible electroosmotic flow. Although closed-form expressions for the solute distribution and coefficient of

dispersion were obtained in that study, the analytical solutions were necessarily based on the Debye-Hückel approximation that the zeta potential at the tube or channel walls is small. While such solutions are valuable in understanding the fundamental phenomena of fluid motion and solute transport in electroosmotic flows, there are many practical applications in which the zeta potential is not negligibly small. Thus, this approximation is not used in the present study. Instead we employ combined analytical and numerical methods to obtain the fluid velocity and a two-term series describing the late-time concentration field for electroosmotic flow at non-negligible zeta potentials. Solutions are presented for both a translating solute interface and a solute peak evolving from an initially planar source of unit strength.

GOVERNING EQUATIONS

Consider the electroosmotic fluid motion and solute transport in a tube or a channel of infinite width. Assuming that the fluid is incompressible and that transport properties are constant, the time-dependent concentration field is governed by

$$\frac{\partial c}{\partial t} + \mathbf{u}\cdot\nabla c = D\nabla^2 c \tag{1}$$

where c is the local solute concentration, t is time, $\mathbf{u} = u\mathbf{i} + v\mathbf{j}$ is the local fluid velocity, and D is the coefficient of diffusion. Further assuming that the flow is steady, that there are no applied pressure gradients and that inertial effects are small, the momentum equation may be written as

$$\mu\nabla^2\mathbf{u} = \rho_e\nabla\phi \tag{2}$$

where μ is the fluid viscosity, ρ_e is the net local charge density, and ϕ is the electric potential. Finally, for a dielectric constant, ϵ, that does not vary with position, the Poisson equation governing the electric potential is

$$\epsilon\,\nabla^2\phi = -\rho_e \tag{3}$$

and the charge density for equivalent ions may be related to the electric potential through the Boltzmann distribution, $\rho_e = -2Fzc_e\sinh(zF\phi/RT)$ where F is the Faraday constant, z is the ion charge number, c_e is the bulk-fluid ion concentration, R is the universal gas constant, and T is the temperature.

We now introduce a set of dimensionless variables. The new normalized dependent variables are taken as $c^* = c/c_o$, $\mathbf{u}^* = \mathbf{u}/U$ and $\phi^* = \phi/\zeta$, where c_o is some reference concentration yet to be specified, U is the mean axial fluid speed spatially averaged across the tube or channel, and ζ is the electric potential at the tube or channel wall. The new independent variables are $x^* = (x - Ut)/a$, $y^* = y/a$ and $t^* = Dt/a^2$, where x and y are the axial and transverse coordinates, and a is the tube radius or channel half-height. This normalization leads to three new parameters, the normalized Debye length,

$$\lambda^{*2} = \left(\frac{\lambda}{a}\right)^2 = \frac{\epsilon RT}{2F^2z^2c_e a^2} \tag{4}$$

the normalized wall potential, $\zeta^* = zF\zeta/RT$, and the Peclet number, $Pe = Ua/D$ indicating the relative magnitudes of advective and diffusive transport rates.

Introducing these normalized variables into the primitive governing equations and rearranging slightly yields

$$\frac{\partial c^*}{\partial t^*} + Pe\left(\mathbf{u}^*\cdot\nabla c^* - \frac{\partial c^*}{\partial x^*}\right) = \nabla^2 c^* \tag{5}$$

$$\beta\,\nabla^2\mathbf{u}^* = -\nabla^2\phi^*\,\mathbf{E}^* \tag{6}$$

and

$$\lambda^{*2}\,\nabla^2\phi^* = \frac{1}{\zeta^*}\sinh(\zeta^*\phi^*) \tag{7}$$

for Eqs. (1), (2) and (3), respectively. The new dependent variable, $\mathbf{E}^* = -\nabla\phi/E_x$ is the electric field vector normalized by the applied axial electric field, E_x. Note that the operators ∇ and ∇^2 above implicitly involve derivatives with respect to the normalized independent variables x^* and y^* when applied to any normalized dependent variable.

The normalization additionally introduces one dimensionless unknown constant, $\beta = -\mu U/\epsilon\zeta E_x$. This constant is the mean axial fluid speed normalized by the Helmholtz-Smoluchowski speed for flow past a plane charged surface. Its value is given by the condition

$$(n+1)\int_0^1 u^* y^{*n} dy^* = 1 \tag{8}$$

in accordance with the definition of the mean fluid speed, U. The parameter n in Eq. (8) is used to describe either the planar or axisymmetric geometries by taking $n=0$ or 1, respectively.

Recognizing that the incompressible flow in a long tube or channel must be one dimensional, and that the radial component of the fluid velocity is

therefore everywhere zero, the diffusion-advection equation (5) may be rewritten as

$$\frac{\partial c^*}{\partial t^*} + Pe(u^*-1)\frac{\partial c^*}{\partial x^*} = \frac{\partial^2 c^*}{\partial x^{*2}} + \frac{1}{y^{*n}}\frac{\partial}{\partial y^*}\left(y^{*n}\frac{\partial c^*}{\partial y^*}\right) \quad (9)$$

where u^* is the normalized fluid speed in the axial direction. Initial and boundary conditions for the normalized solute concentration are given in Appendix A.

Now recognizing that the second derivative of the electric potential in the axial direction is small compared to that in the transverse direction, and that the normalized electric field is defined such that $\mathbf{E}^* \cdot \mathbf{i} = 1$, the axial component of the momentum equation (6) may be written as

$$\frac{\beta}{y^{*n}}\frac{d}{dy^*}\left(y^{*n}\frac{du^*}{dy^*}\right) = -\frac{1}{y^{*n}}\frac{\partial}{\partial y^*}\left(y^{*n}\frac{\partial \phi^*}{\partial y^*}\right) \quad (10)$$

and the Poisson-Boltzmann equation becomes

$$\frac{\lambda^{*2}}{y^{*n}}\frac{\partial}{\partial y^*}\left(y^{*n}\frac{\partial \phi^*}{\partial y^*}\right) = \frac{1}{\zeta^*}\sinh(\zeta^*\phi^*) \quad (11)$$

Boundary conditions for the fluid velocities are $du^*/dy^* = 0$ at $y^* = 0$ and $u^* = 0$ at $y^* = 1$. Those for the electric potential are $\partial\phi^*/\partial y^* = 0$ at $y^* = 0$ and $\phi^* = 1$ at $y^* = 1$.

Given the governing equation (10) and parallels between the u^* and ϕ^* boundary conditions, we see that the normalized fluid velocity can be expressed directly in terms of the normalized electric potential as

$$u^* = \frac{1-\phi^*}{\beta} \quad (12)$$

Substituting this result into Eq. (8), the normalized mean fluid speed may be written explicitly as

$$\beta = -\frac{\mu U}{\epsilon \zeta E_x} = (n+1)\int_0^1 (1-\phi^*)\, y^{*n} dy^* \quad (13)$$

Note that ϕ^* here implicitly represents only the intrinsic portion of the electric potential, as described by Eq. (11). The fluid velocity thus possesses no axial variation due to the applied electric field.

METHOD OF SOLUTION

To solve Eq. (9), we now introduce one more transformation of the axial coordinate, $\eta = x^*/2\sqrt{t^*}$. Introducing this new variable into the diffusion-advection equation yields

$$\frac{\partial^2 c^*}{\partial \eta^2} + 2\eta\frac{\partial c^*}{\partial \eta} = 2\sqrt{t^*}Pe(u^*-1)\frac{\partial c^*}{\partial \eta} + 4t^*\left[\frac{\partial c^*}{\partial t^*} - \frac{1}{y^{*n}}\frac{\partial}{\partial y^*}\left(y^{*n}\frac{\partial c^*}{\partial y^*}\right)\right] \quad (14)$$

In a previous analysis, we showed that Eq. (14) possesses a late-time solution of the form

$$c^* t^{*m/2} = f_0 + \frac{1}{2\sqrt{t^*}}\left(f_1 + Pe\frac{df_0}{d\eta}g_1\right) + \frac{1}{4t^*}\left(f_2 + Pe\frac{df_1}{d\eta}g_1 + Pe^2\frac{d^2 f_0}{d\eta^2}g_2\right) + \ldots \quad (15)$$

where the functions g_j depend only on the transverse position, y^*, and the functions f_k depend only on the transformed axial position, η. Values of the parameter $m = 0$ or $m = 1$ identify the cases of a translating interface or instantaneous source, respectively.

Substituting Eq. (15) into Eq. (14), grouping like powers of time, and separating the results into functions of the axial and transverse directions yields governing equations for the functions f_k and g_j. For the first few terms these are

$$(1+\alpha_0 Pe^2) f_0'' + 2\eta f_0' + 2m f_0 = 0 \quad (16)$$

$$(1+\alpha_0 Pe^2) f_1'' + 2\eta f_1' + 2(m+1) f_1 = -\alpha_1 Pe^3 f_0''' \quad (17)$$

and

$$g_1'' + n\frac{g_1'}{y^*} - (u^*-1) = 0 \quad (18)$$

$$g_2'' + n\frac{g_2'}{y^*} - (u^*-1)\, g_1 = \alpha_0 \quad (19)$$

$$g_3'' + n\frac{g_3'}{y^*} - (u^*-1)\, g_2 - \alpha_0 g_1 = \alpha_1 \quad (20)$$

Note that primes applied to the functions f_k denote differentiation with respect to η, while those applied to g_j denote differentiation with respect to y^*. The separation constants or eigenvalues α_0 and α_1 are yet to be determined.

Boundary conditions for the functions f_k are given in Appendix A for the cases of a traveling interface and an instantaneous planar source. Based on symmetry about the centerline and the condition of zero solute flux through the tube or channel walls, boundary conditions for the functions g_1 and g_2 are $g_1'(0) = g_1'(1) = g_2'(0) = g_2'(1) = 0$. In addition, these functions must satisfy

$$\bar{g}_j = (n+1)\int_0^1 g_j\, y^{*n} dy^* = 0 \quad (21)$$

for all j in order that all axial variation of the concentration field is carried by the functions f_k alone.

Because the governing equations (18-20) are second order, only one constant of integration is available to satisfy the two boundary conditions on the derivative $g_j'(y^*)$. As a result, one of the two boundary conditions can be satisfied only by appropriate choices for the eigenvalues, α_k. From the governing equation (18) and condition $g_1'(0)=0$, the derivative $g_1'(1)$ at the tube or channel wall can be written as

$$g_1'(1) = \int_0^1 (u^* - 1)\, y^{*n} dy^* \equiv 0 \qquad (22)$$

By Eq. (8), the first-order solution therefore automatically satisfies all required conditions and so imposes no constraint on either α_0 or α_1. For the higher-order terms, however, the conditions $g_2'(1)=0$ and $g_3'(1)=0$ require that

$$\alpha_0 = -(n+1) \int_0^1 [(u^* - 1)\, g_1]\, y^{*n} dy^* \qquad (23)$$

and

$$\alpha_1 = -(n+1) \int_0^1 [(u^* - 1)\, g_2 + \alpha_0 g_1]\, y^{*n} dy^* \qquad (24)$$

respectively. These eigenvalues are thus uniquely determined by the two boundary conditions $g_j'(0)=g_j'(1)=0$. The two constants of integration for each function g_j are then determined by the integral constraint (21) and the condition $g_j'(0)=0$. Note that the term $\alpha_0 g_1$ in Eq. (24) arises naturally in the derivation of this expression from Eq. (20), but by Eq. (21) it does not contribute to the integral.

Although this method of solution was derived for electroosmotic flow, it is more broadly applicable to any parallel flow in a tube or channel. In Appendix C, we apply this approach to the classic Taylor problem of late-time solute transport in pressure-driven flows. The zeroth-order solution yields Taylor's result for the coefficient of dispersion, while the first-order solution describes the approach to this late-time asymptote.

NUMERICAL PROCEDURE

As discussed later, Eqs. (16) and (17) describing the axial variation of the solute concentration possess closed-form analytical solutions. Equation (11), however, possesses no such solution for the electric potential in a tube or channel of finite width and non-negligible values of ζ^*. In general, Eq. (11) and the dependent equations describing the fluid velocity and transverse variation of the solute concentration must be solved numerically. For this we employ a very accurate shooting technique based on the following procedure.

Given values of λ^* and ζ^*, Eq. (11) is first integrated from $y^*=0$ to $y^*=1$ using the boundary condition $\phi^{*\prime}(0)=0$ and an initial guess for $\phi^*(0)$. The resulting value of $\phi^*(1)$ does not necessarily satisfy the required boundary condition $\phi^*(1)=1$, so an improved value of $\phi^*(0)$ is computed based on the discrepancy between the observed and required boundary values. This process in repeated to convergence, each time using the improved estimate of $\phi^*(0)$ to begin the integration. These integrations are performed using a double-precision routine, DDERKF [4], with specified relative and absolute error tolerances of 10^{-12} and 10^{-20}, respectively. New values of $\phi^*(0)$ are computed automatically using the nonlinear algebraic equation solver DNSQE [4]. The convergence criterion for the results shown here is a relative error of 10^{-8} in the value of $\phi^*(0)$. This criterion yields an error below 10^{-6} in satisfying the boundary condition $\phi^*(1)=1$.

Once the electric potential is known, the corresponding value of β is computed from Eq. (13). The required quadrature is performed by integrating Eqs. (11) and (13) together as a coupled pair, using the correct value of $\phi^*(0)$ previously determined. From Eq. (12), the velocity profile is then known. Next, Eqs. (18), (19), (21), (23) and (24) are added to the system of equations and integrated along with Eqs. (11) and (13) to yield $g_1(y)$, $g_2(y)$, α_0 and α_1. This final system of equations consists of ten coupled, first-order ordinary differential equations. These are again integrated by means of DDERKF, using the relative and absolute error tolerances described above.

To satisfy the integral constraints imposed by Eq. (21), the system of equations is simply integrated multiple times. During the first integration, the unknown value $g_1(0)$ is taken as zero and the equations are integrated from $y^*=0$ to $y^*=1$, yielding a tentative value of $\bar{g}_1$ from Eq. (21). The integration is then repeated, this time setting $g_1(0)=-\bar{g}_1$. By this method Eq. (21) is satisfied exactly. Once $g_1(y)$ is known, the system of equations is integrated again, with $g_2(0)=0$, to yield α_0 and a tentative value of $\bar{g}_2$. One more integration, setting $g_2(0)=-\bar{g}_2$, gives $g_2(y)$ satisfying Eq. (21). A final integration yields α_1.

This numerical procedure was checked against previously-published analytical solutions describing the electric potential in a tube for $\zeta^*=2.7$ and several values of λ^* between 0.01 and 10 [5]. The two results agree within the accuracy of reading the ear-

lier plots. The present results show similarly good agreement with previous analytical solutions based on inner and outer expansions for ζ^* between 0 and 10 and λ^* between 0.01 and 1 [6]. The procedure was further benchmarked against known analytical solutions describing the electric potential for negligibly small ζ^* in both tubes and channels [3]. In those cases, the two results agree within a relative error of 10^{-6} for all values of y^* and values of λ^* between 10^{-3} and 10^3. Finally, computed values of α_0, α_1, $g_1(y)$ and $g_2(y)$ were compared with known analytical solutions for a parabolic profile of the fluid speed [7,8,9]. Such a profile arises in the limit $\lambda^* \to \infty$. The numerical solutions reproduce these analytical results within relative errors of 10^{-6} for both tube and channel geometries.

The shooting procedure described above works well when λ^* is greater than about 10^{-3}. For smaller values, the shooting target becomes difficult to hit since very small changes in $\phi^*(0)$ then yield large changes in $\phi^*(1)$. This sensitivity results from parasitic solutions to Eq. (11) that grow exponentially in y^*. The rate of this growth increases with decreasing λ^*. Still worse, such exponential growth can lead to a numerical overflow before reaching the target loaction, $y^* = 1$, unless $\phi^*(0)$ is very close to the correct value. Integrating Eq. (11) backwards from $y^* = 1$ helps to solve this problem, but introduces new problems of comparable severity. Because of these difficulties, an alternate method is employed when λ^* is very small.

When λ^* is small, the electric potential varies only in a region close to the tube or channel wall. The boundary condition $\phi^{*\prime}(0) = 0$ becomes nearly superfluous in this limit, and the electric potential can be well approximated by [10]

$$\phi^* \sim \frac{4}{\zeta^*} \operatorname{arctanh}\left[e^{(y^*-1)/\lambda^*} \tanh\left(\frac{\zeta^*}{4}\right)\right] \qquad (25)$$

as $\lambda^* \to 0$. This is an exact solution to Eq. (11) for all ζ^* and satisfies the boundary condition $\phi^*(1) = 1$. It is approximate only in the sense that the condition $\phi^{*\prime}(0) = 0$ is not satisfied exactly except in the limit $\lambda^* \to 0$. In practice, however, this solution is very accurate for all λ^* less than about 0.01. Shooting is thus unnecessary when λ^* is small, and the electric potential can be described instead by this closed-form result. The values of $g_1(y)$, $g_2(y)$, α_0 and α_1 in this alternate method are still computed by the balance of the numerical procedure described above since all of the required integrals of ϕ^*, as expressed by Eq. (25), are not known in analytical form.

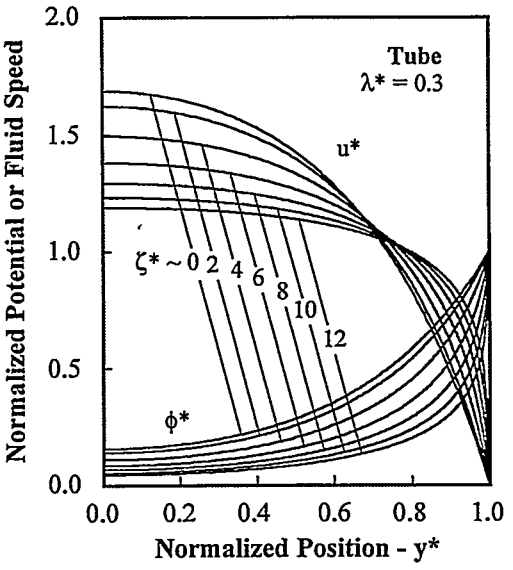

Figure 1. Normalized electric potential (ϕ^*) and normalized fluid speed (u^*) for electroosmotic flow in a tube at non-negligible zeta potentials.

FLUID MOTION IN A TUBE

The computed normalized electric potential and axial fluid speed are shown in Fig. 1 for electroosmotic flow in a tube. These sample results are for $\lambda^* = 0.3$ and a range of values of ζ^*. Here we see that increasing ζ^* is somewhat analogous to decreasing λ^*. In both cases, the electric potential and fluid velocity develop a steeper gradient near the tube wall, but then exhibit an increased region of nearly uniform values near the centerline. We thus expect that increased ζ^* will yield more uniform concentration fields and reduced late-time solute dispersion.

Figure 2 shows computed values of the normalized mean fluid speed, β, corresponding to the conditions of Fig. 1. Here we see that increasing ζ^* always increases β. This is again because larger ζ^* yields an effectively smaller Debye layer thickness and so yields a normalized electric potential closer to zero over a broader portion of the tube cross-section. By Eq. (13), β is thus increased. We also see that β approaches unity as λ^* becomes small and falls as $1/\lambda^{*2}$ for all ζ^* as λ^* grows large.

In addition to numerical results like those of Figs. (1) and (2), we have obtained analytical solutions for the fluid velocity in the extremes of small and large λ^*. Such solutions serve to quantify the general observations above and further provide

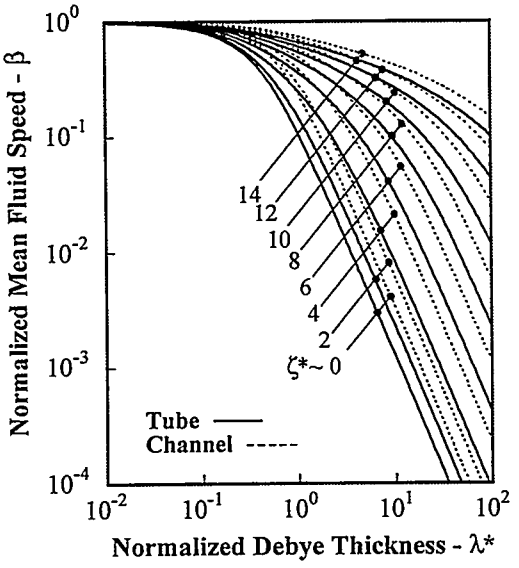

Figure 2. Normalized mean fluid speed for electroosmotic flow in a tube (solid) and channel (dashed) at non-negligible zeta potentials.

valuable benchmark results for testing more general finite-difference and finite-element methods. Recall from Eq. (12) that the local fluid speed under all conditions is given by $u^* = (1 - \phi^*)/\beta$. Thus local axial fluid speeds, u^*, are uniquely determined by specifying only the normalized electric potential, ϕ^*, and the normalized mean axial fluid speed, β. These are given below in analytical form for small and large λ^*.

In the important practical limit of small λ^*, the electric potential is given by Eq. (25) and the corresponding normalized mean fluid speed is

$$\beta \sim 1 - \frac{4\lambda^*}{\zeta^*}\left[\mathrm{Li}_2(\xi) - \mathrm{Li}_2(-\xi)\right] \quad \text{as} \quad \lambda^* \to 0 \quad (26)$$

where $\xi = \tanh(\zeta^*/4)$ and $\mathrm{Li}_2(\xi)$ is the dilogarithm function,

$$\mathrm{Li}_2(\xi) = -\int_0^{\xi} \ln(1-s)\frac{ds}{s} = \sum_{k=1}^{\infty} \frac{\xi^k}{k^2} \qquad (27)$$

This result, correct to order λ^*, was obtained by integrating Eq. (25) in accordance with Eq. (13) defining the normalized mean fluid speed. It agrees with the value of β computed numerically within 5% for all ζ^* when λ^* is less than 0.5; when λ^* is less than 0.2, the two agree within 1%.

The asymptotic behavior of Eq. (25) in the limit of small ζ^* is

$$\phi^* \sim e^{(y^*-1)/\lambda^*}\left(1 - \frac{\zeta^{*2}}{48}\left[1 - e^{2(y^*-1)/\lambda^*}\right]\right) \quad (28)$$

as $\lambda^* \to 0$ and $\zeta^* \to 0$. The corresponding normalized axial speed in this double limit is

$$\beta \sim 1 - 2\lambda^*\left(1 - \frac{\zeta^{*2}}{72}\right) \quad \text{as} \quad \lambda^* \to 0,\ \zeta^* \to 0 \quad (29)$$

This expression for β is consistent with our previous result [3] of $\beta = 1 - 2\lambda^* I_1(1/\lambda^*)/I_0(1/\lambda^*) \sim 1 - 2\lambda^*$ for the case of vanishingly small ζ^*. The values of $1-\beta$ computed using Eq. (29) agree with those of Eq. (26) within 3% for $\zeta^* \le 2$ and within 15% for $\zeta^* \le 4$. Note that the mean normalized fluid speed varies weakly with ζ^* when ζ^* is small. The term $\zeta^{*2}/72$ yields a correction to $1 - \beta$ of only about 5% for $\zeta^* = 2$. Thus by Eq. (13), the dimensional mean fluid speed should grow about linearly with ζ for small ζ^* when λ^* is small.

In the alternate extreme of large ζ^*, the asymptotic behavior of Eq. (25) is

$$\phi^* \sim -\frac{2}{\zeta^*}\ln\left[\mathrm{sech}^2\left(\frac{y^*-1}{2\lambda^*}\right)e^{-\zeta^*/2} - \tanh\left(\frac{y^*-1}{2\lambda^*}\right)\right] \quad (30)$$

as $\lambda^* \to 0$ and $\zeta^* \to \infty$. This yields a corresponding normalized mean fluid speed of

$$\beta \sim 1 - \lambda^*\frac{\pi^2}{\zeta^*} \quad \text{as} \quad \lambda^* \to 0,\ \zeta^* \to \infty \qquad (31)$$

This expression for β can be obtained directly from Eq. (26) since $\xi \to 1$ as $\zeta^* \to \infty$ and $\mathrm{Li}_2(1) - \mathrm{Li}_2(-1) = \pi^2/4$. Values of $1-\beta$ computed using Eq. (31) agree with those of Eq. (26) within 3% for $\zeta^* \ge 10$, and within 1% for $\zeta^* \ge 14$.

Analytical solutions to Eqs. (11) and (13) can also be obtained in the limit of large λ^*. In this extreme, the potential and normalized mean fluid speed are

$$\phi^* \sim 1 - \frac{\sinh\zeta^*}{4\zeta^*\lambda^{*2}}(1 - y^{*2}) \quad \text{as} \quad \lambda^* \to \infty \qquad (32)$$

and

$$\beta \sim \frac{1}{8\lambda^{*2}}\frac{\sinh\zeta^*}{\zeta^*} \quad \text{as} \quad \lambda^* \to \infty \qquad (33)$$

These expressions were obtained by solving Eq. (11) for large λ^* using a perturbation expansion in $1/\lambda^*$ and then using the resultant electric potential to compute β from Eq. (13). As a result, they carry the

additional restriction that $\sinh\zeta^*/\zeta^* \ll \lambda^{*2}$. Equation (33) reproduces the values of β determined numerically within about 2% for all $\lambda^* \geq 3$, provided that $\sinh\zeta^*/\zeta^* < \lambda^{*2}/50$. Note that the fluid velocity in this limit of large λ^* recovers the expected parabolic profile $u^* = (1-\phi^*)/\beta = 2(1-y^{*2})$ for pressure-driven flow in a tube.

The asymptotic behavior of Eq. (33) for small values of ζ^* is

$$\beta \sim \frac{1}{8\lambda^{*2}}\left(1+\frac{\zeta^{*2}}{6}\right) \quad \text{as} \quad \lambda^* \to \infty,\ \zeta^* \to 0 \quad (34)$$

Again this is consistent with the result $\beta = 1 - 2\lambda^* I_1(1/\lambda^*)/I_0(1/\lambda^*) \sim 1/8\lambda^{*2}$ for $\lambda^* \to \infty$ and $\zeta^* = 0$. The expansion of Eq. (33) for large ζ^* is

$$\beta \sim \frac{1}{8\lambda^{*2}}\frac{e^{\zeta^*}}{2\zeta^*} \quad \text{as} \quad \lambda^* \to \infty,\ \zeta^* \to \infty \quad (35)$$

We note that the effect of ζ^* on the normalized mean fluid speed at large λ^* is much stronger than it is when λ^* is small. This is especially the case as ζ^* becomes large. In this limit, the dimensional fluid speed increases exponentially with increasing ζ so long as $e^{\zeta^*}/2\zeta^*$ remains much smaller than λ^{*2}.

FLUID MOTION IN A CHANNEL

Results paralleling those of Fig. 1 for a tube are shown for a channel in Fig. 3. Normalized mean fluid speeds for flow in a channel appear in the previous Fig. 2 as dashed curves. These results are very similar to those for a tube, except that β for a channel is everywhere a bit higher than that for a tube at the same values of λ^* and ζ^*.

As for a tube, local fluid speeds in a channel are given by $u^* = (1-\phi^*)/\beta$. The flow field is thus again determined uniquely by the normalized electric potential, ϕ^*, and normalized mean speed, β.

In the limit $\lambda^* \to 0$, the electric potential given in Eq. (25) applies equally to a tube and a channel since the Debye layer thickness is then very small compared to the tube diameter or channel width. Despite this, the value of β differs between the two geometries owing to the difference in Eq. (13) for the two cases. For a channel, the normalized mean fluid speed for small λ^* is

$$\beta \sim 1 - \frac{2\lambda^*}{\zeta^*}\left[\mathrm{Li}_2(\xi) - \mathrm{Li}_2(-\xi)\right] \quad \text{as} \quad \lambda^* \to 0 \quad (36)$$

where again $\xi = \tanh(\zeta^*/4)$ and $\mathrm{Li}_2(\xi)$ is the dilogarithm function given by Eq. (27). As before, this

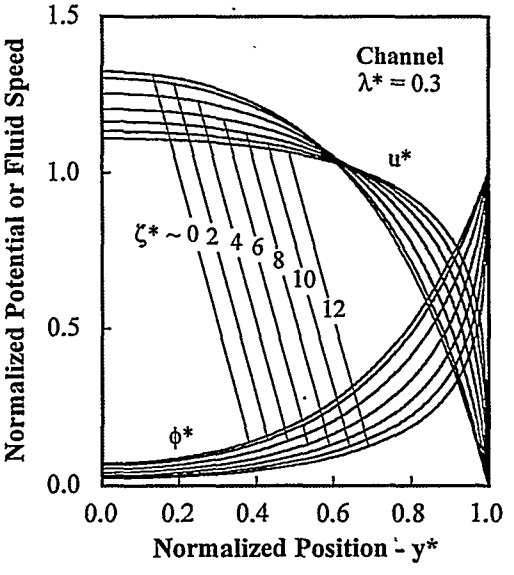

Figure 3. Normalized electric potential (ϕ^*) and normalized fluid velocity (u^*) for electroosmotic flow in a channel.

result was obtained using the analytical expression for the electric potential given by Eq. (25). The accuracy and applicable range of this result are comparable to the parallel result for a tube, given by Eq. (26).

In the limit of small λ^* and small ζ^*, the electric potential in a channel is again the same as that in a tube and is given by Eq. (28). The corresponding asymptotic behavior of Eq. (36) in this small ζ^* limit is

$$\beta \sim 1 - \lambda^*\left(1 - \frac{\zeta^{*2}}{72}\right) \quad \text{as} \quad \lambda^* \to 0,\ \zeta^* \to 0 \quad (37)$$

This expression for a channel is again consistent with our previous solution $\beta = 1 - \lambda^* \tanh(1/\lambda^*) \sim 1 - \lambda^*$ for vanishing ζ^* [3]. The asymptotic behavior of Eq. (36) at large ζ^* is

$$\beta \sim 1 - \lambda^*\frac{\pi^2}{2\zeta^*} \quad \text{as} \quad \lambda^* \to 0,\ \zeta^* \to \infty \quad (38)$$

The corresponding potential in this limit is again given by Eq. (30), which applies to both the tube and channel geometries when λ^* is small. The accuracy and applicable range of Eqs. (37) and (38) are comparable to those of the corresponding results for a tube.

Analytical solutions to Eqs. (11) and (13) have also been obtained for flow in a channel at large λ^*. In this case, the results are

$$\phi^* \sim 1 - \frac{\sinh\zeta^*}{2\lambda^{*2}\zeta^*}(1-y^{*2}) \quad \text{as} \quad \lambda^* \to \infty \qquad (39)$$

and

$$\beta \sim \frac{1}{3\lambda^{*2}}\frac{\sinh\zeta^*}{\zeta^*} \quad \text{as} \quad \lambda^* \to \infty \qquad (40)$$

As with Eqs. (32) and (33), these results were obtained by solving Eq. (11) for large λ^* using a perturbation expansion and so again carry the restriction that $\sinh\zeta^*/\zeta^* \ll \lambda^{*2}$. Equation (40) reproduces the numerically-determined values of β within about 4% for all $\lambda^* \geq 4$ provided that $\sinh\zeta^*/\zeta^* < \lambda^{*2}/100$. Note that these expressions recover the parabolic profile $u^* = (1-\phi^*)/\beta = 3(1-y^{*2})/2$ for pressure-driven flow in a channel.

The asymptotic behavior of Eq. (40) for small values of ζ^* is

$$\beta \approx \frac{1}{3\lambda^{*2}}\left(1+\frac{\zeta^{*2}}{6}\right) \quad \text{as} \quad \lambda^* \to \infty,\ \zeta^* \to 0 \qquad (41)$$

Again, this is consistent with $\beta = 1-\lambda^*\tanh(1/\lambda^*) \sim 1/3\lambda^{*2}$ for $\lambda^* \to \infty$ and $\zeta^* = 0$. The corresponding expansion of Eq. (40) for large ζ^* is

$$\beta \sim \frac{1}{3\lambda^{*2}}\frac{e^{\zeta^*}}{2\zeta^*} \quad \text{as} \quad \lambda^* \to \infty,\ \zeta^* \to \infty \qquad (42)$$

The additional restriction that $\sinh\zeta^*/\zeta^* \ll \lambda^{*2}$ also applies here.

AXIAL VARIATION OF THE CONCENTRATION FIELD

The axial variation of the mean solute concentration, spatially averaged across the tube or channel cross-section, is governed by Eqs. (16) and (17). These equations were previously solved [3], subject to the initial and boundary conditions outlined in Appendix A. For the case of a translating interface, $m=0$, the results are

$$f_0 = \frac{1}{2}\operatorname{erfc}\eta' \qquad (43)$$

and

$$f_1 = \frac{\alpha_1 Pe^3}{2\sqrt{\pi\left(1+\alpha_0 Pe^2\right)^3}}\left(1-2\eta'^2\right)e^{-\eta'^2} \qquad (44)$$

where

$$\eta' = \frac{\eta}{\sqrt{1+\alpha_0 Pe^2}} \qquad (45)$$

For the case of an instantaneous planar source of unit strength, $m=1$, the zeroth and first-order functions are

$$f_0 = \frac{1}{2\sqrt{\pi\left(1+\alpha_0 Pe^2\right)}}e^{-\eta'^2} \qquad (46)$$

and

$$f_1 = \frac{\alpha_1 Pe^3}{2\sqrt{\pi}\left(1+\alpha_0 Pe^2\right)^2}\left(3-2\eta'^2\right)\eta' e^{-\eta'^2} \qquad (47)$$

where η' is again given by Eq. (45). The applicability of these expressions is discussed in Appendix B.

Noting the definition of η given above, we see that Eqs. (43) and (46) describe a diffusion process in which the molecular diffusivity, D, is replaced by an effective diffusivity $D' = D\left(1+\alpha_0 Pe^2\right)$. The eigenvalue α_0 is thus equivalent to the more familiar coefficient of dispersion. Similarly, the eigenvalue α_1 is also equivalent to the coefficient of skewness.

The solutions for f_0 and f_1 describing the axial variation of the concentration field are applicable to both the tube and channel geometries and to all profiles of the fluid velocity. The geometry and velocity distribution influence these solutions only through the eigenvalues α_0 and α_1, which are determined by solving the equations describing the transverse variation of the solute concentration.

TRANSVERSE VARIATION OF THE CONCENTRATION FIELD

Figure 4 shows computed values of the function $g_1(y^*)$ describing the first-order term of the transverse variation of the concentration field. These results are useful in understanding the effects of a nonuniform fluid velocity on the concentration field.

Recall from Eq. (15) that the late-time concentration field is given by $c^* t^{*m/2} = f_0 + (f_1 + Pe\, f_0' g_1)/2\sqrt{t^*} + O[1/t^*]$. Thus the function g_1 in the concentration field is multiplied by both the Peclet number and the derivative of f_0. For the case of a moving interface having a high concentration on the trailing side, the derivative of f_0 is everywhere negative. Thus from Fig. 4 we see that the electroosmotic velocity profile increases the concentration on the tube centerline, $y^* = 0$, at all axial positions. Likewise, the concentration at the tube wall is everywhere reduced. For the case of an instantaneous source, however, the derivative of f_0 is positive for $\eta < 0$ and negative for $\eta > 0$. In this case, concentrations on the centerline are reduced behind the mid-plane of the solute peak, but are antisymmetrically increased on the centerline ahead. Concen-

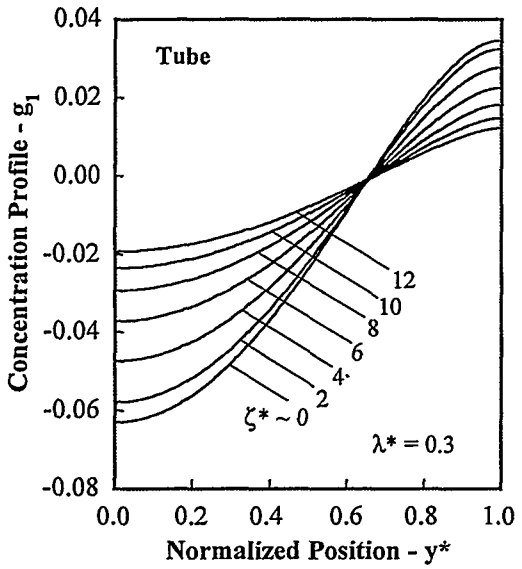

Figure 4. First-order correction describing the transverse variation in solute concentration for electroosmotic flow in a channel.

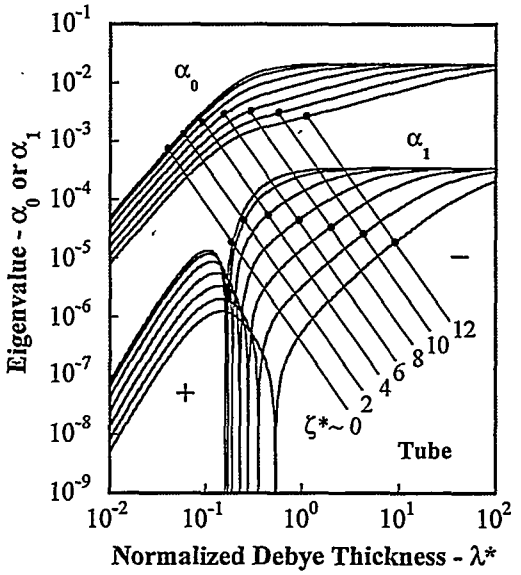

Figure 5. Eigenvalues for flow in a tube. First-order eigenvalue α_0 is the coefficient of dispersion; α_1 is coefficient of skewness.

trations at the tube walls exhibit just the opposite behavior. We also see in Fig. 4 that increasing values of the zeta potential tend to reduce the transverse variation of the concentration field. This is consistent with the previous observation that increasing ζ^* produces a more uniform fluid velocity over a large central portion of the tube cross-section.

Computed values of α_0 and α_1 are shown in Fig. (5). These values along with Eqs. (43) through (47) provide the complete two-term solution describing axial variation of the mean concentration field in the late-time limit. Here we see that α_0 is positive for all values of λ^* and ζ^*, and that increasing ζ^* always decreases its value. Since α_0 is the same as the coefficient of dispersion, solute dispersion is thus reduced when ζ^* is increased. This is again due to the fact that increasing ζ^* produces a steeper gradient of the fluid velocity at the tube wall, but also gives a more uniform velocity near the centerline.

Increasing ζ^* also decreases the magnitude of α_1 for all λ^*, which by Eqs. (44) and (47) reduces the late-time skewness of the mean solute concentration. Note that values of α_1 are negative on the right of Fig. 5, but become positive below some critical value of λ^* that depends on ζ^*. For the problem of a translating solute interface, the centroid of the mean concentration field is thus shifted forward of its asymptotic position for small values of λ^*, but is shifted rearward of this position for large λ^*. The centroid of the concentration field is similarly shifted from its asymptotic position for the case of an instantaneous planar source. For the special case in which α_1 vanishes, the late-time solutions exhibit no asymmetry except that due to still higher-order terms.

Although the eigenvalues in Fig. 5 exhibit a complex dependence on λ^* and ζ^*, they follow well defined asymptotes in the limits of both small and large λ^*. When λ^* is large, the charge distribution and electric potential are nearly uniform across the tube. In this case, the applied electric field produces a nearly uniform body force that acts on the fluid in manner analogous to the pressure gradient in pressure-driven flows. The result in both cases is a parabolic profile of the fluid velocity, having a maximum speed of two that occurs on the centerline of the tube. In this limit of large λ^*, our present solutions recover the well-known results of Taylor [7] and Chatwin [9] for pressure-driven flow in a tube. These are

$$\alpha_0 \sim \frac{1}{48} \quad \text{and} \quad \alpha_1 \sim -\frac{1}{2880} \quad \text{as} \quad \lambda^* \to \infty \quad (48)$$

The applicable range of these results is $\lambda^* > 2$ and $\zeta^{*2} < \lambda^*$. Over this range, the discrepancy between

Eq. (48) and the numerical results of Fig. 5 is less than 2% for α_0 and less than 3% for α_1.

In most practical applications of electroosmotic flow, the normalized Debye length is very small. In the limit, the results of Fig. 5 can be expressed as

$$\alpha_0 \sim \frac{1}{2}\lambda^{*2} h_0 \quad \text{as} \quad \lambda^* \to 0 \tag{49}$$

where the factor $\lambda^{*2}/2$ is the asymptotic value of α_0 for $\lambda^* \to 0$ and negligible ζ^* [3]. The function h_0 depends only on ζ^* and is well-approximated by

$$h_0 \approx \frac{2592 + 24\zeta^{*2}}{2592 + 96\zeta^{*2} + \zeta^{*4}} \tag{50}$$

This function is an empirical fit to the numerical results of Fig. 5, taking into account the asymptotic behavior at small and large values of ζ^*. These limiting behaviors are $h_0 = 1 - \zeta^{*2}/36$ as $\zeta^* \to 0$, and $h_0 = \pi^4/4\zeta^{*2} \approx 24/\zeta^{*2}$ as $\zeta^* \to \infty$. Equation (49), with h_0 given by Eq. (50), agrees with the numerical results within 4% for values of λ^* less than 0.01 and all values of ζ^*.

The behavior of α_1 in the limit of small λ^* similarly can be expressed as the product of the solution for $\zeta^* \to 0$ and a function accounting for the effect of non-negligible ζ^*. In this case, the result is

$$\alpha_1 \sim \frac{1}{12}\lambda^{*3} h_1 \quad \text{as} \quad \lambda^* \to 0 \tag{51}$$

where

$$h_1 \approx \frac{5760 + 120\zeta^{*2}}{5760 + 360\zeta^{*2} + 12\zeta^{*3} + \zeta^{*4} + \zeta^{*5}} \tag{52}$$

As with h_0, the function h_1 represents an empirical fit to the numerical results. Here the asymptotic behaviors are $h_1 = 1 - \zeta^{*2}/24$ as $\zeta^* \to 0$, and $h_1 = \pi^6/8\zeta^{*3} \approx 120/\zeta^{*3}$ as $\zeta^* \to \infty$. The applicable range of Eq. (51) is again roughly $\lambda^* < 0.01$. For all smaller λ^* and all ζ^*, Eqs. (51) and (52) yield values for α_1 that are within 20% of the values computed numerically. This relative error falls to 2% for $\lambda^* < 0.001$. In this latter range, all inaccuracy in Eq. (51) is attributable to the approximation $\pi^6/8 \approx 120$ in the expression for h_1.

Results describing transverse variation of the concentration field in a channel closely parallel those for a tube presented above. Figure 6 shows computed values of the function $g_1(y^*)$ for $\lambda^* = 0.3$ and values of ζ^* between 0 and 12. We see that the behavior of this function is qualitatively very similar to that shown in Fig. 4 for a tube. The main difference is that the intercept $g_1(y^*) = 0$, indicating

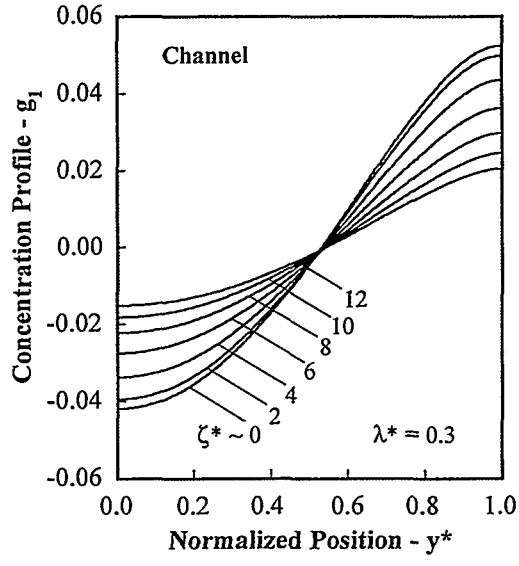

Figure 6. First-order correction describing the transverse variation in solute concentration for electroosmotic flow in a channel.

a neutral point at which the solute concentration is neither increased nor reduced, is shifted closer to the midpoint between the centerline and wall for the case of a channel. This occurs because of the constraint $\bar{g}_1 = 0$ given by Eq. (21). The radial geometry of the tube shifts this neutral point towards the wall, close to the median of the cross-section area, while the planar geometry of the channel requires that the neutral point occur somewhat near the midpoint for any function that is reasonably antisymmetric about the intercept. The previous comments concerning regions of solute enrichment and reduction apply also to the channel geometry.

The eigenvalues α_0 and α_1 for a channel are shown in Fig. 7. These were computed using the same numerical procedure previously described for a tube. We see that the two geometries yield very similar results for α_0, but that α_1 differs significantly between the two. In the case of the tube, this coefficient of skewness changes signs from positive to negative in the vicinity of $\lambda^* = 1$. The results for a channel show no such behavior; α_1 is everywhere positive.

In the limit $\lambda^* \to \infty$, the values of α_0 shown in Fig. 7 recover the known coefficient of dispersion for pressure-driven flow in a channel of infinite width [9]. We find no published record of α_1, the coefficient of skewness, for this geometry. These

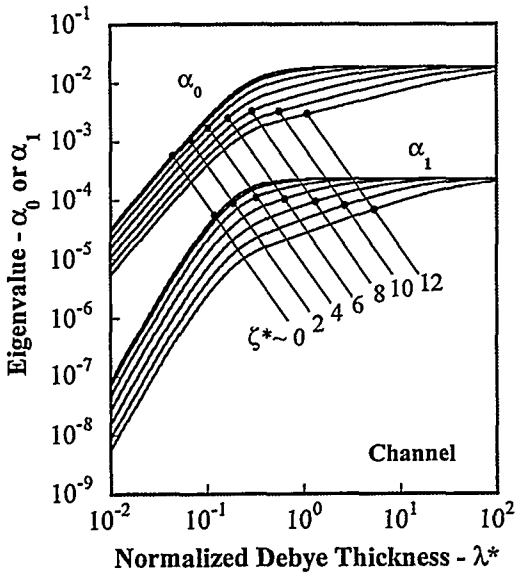

Figure 7. First and second-order eigenvalues for flow in a channel. Increasing ζ^* always reduces these coefficients of dispersion and skewness.

asymptotic values for the channel are

$$\alpha_0 \sim \frac{2}{105} \quad \text{and} \quad \alpha_1 \sim \frac{4}{17325} \quad \text{as} \quad \lambda^* \to \infty \tag{53}$$

In the opposing limit of small λ^*, we find that the eigenvalues for a channel are

$$\alpha_0 \sim \frac{1}{3}\lambda^{*2} h_0 \quad \text{as} \quad \lambda^* \to 0 \tag{54}$$

and

$$\alpha_1 \sim \frac{4}{45}\lambda^{*3} h_1 \quad \text{as} \quad \lambda^* \to 0 \tag{55}$$

where h_0 and h_1 are the same as those given above for a tube.

The functions h_0 and h_1 are the same for both the tube and channel geometries because they apply only in the limit of very small λ^*. In this limit, both geometries appear to be planar over the small region in which the electric potential varies. The fluid velocities in the two geometries are thus the same in this limit, at least within a constant, and the values of α_0 and α_1 must therefore share the same dependence on ζ^* for the two geometries.

SUMMARY

We have examined the electroosmotic fluid motion and late-time solute transport in a tube and in a channel for cases in which the zeta potential is not negligibly small. Using both numerical and analytical methods, the transverse variation of the electric potential and fluid speed were computed over a broad range of the normalized Debye layer thickness, λ^*, and the normalized zeta potential, ζ^*. These fluid velocities were then used to compute the late-time distribution of a neutral non-reacting solute carried in the flow.

The numerical procedure used here is based on a shooting method. This procedure was checked against previously-published analytical and numerical solutions for both large and small values of the zeta potential. In comparisons with analytical results for a negligible zeta potential, the two agree within a relative error of 10^{-6} for all values of the transverse position and values of λ^* between 10^{-3} and 10^3.

Analytical solutions were also obtained for the fluid velocity in a tube and channel in the asymptotic limits of small and large λ^*. The first of these applies when the Debye layer thickness is small compared to the transverse tube or channel dimension and is valid for all values of the normalized zeta potential. The second is applicable to large values of the Debye layer thickness. These solutions are again valid for all ζ^*, but carry the restriction that $\sinh\zeta^*/\zeta^* < \lambda^{*2}$. The accuracy and applicable range of each solution is discussed, and expansions of the solutions for large and small ζ^* are provided.

Based on these fluid velocities and a series describing the full late-time concentration field, the mean axial variation of the field was determined in closed form. The first and second-order solutions describing this variation contain two unknown constants that arise as eigenvalues in the series solution. These eigenvalues are the coefficients of axial dispersion and skewness. They are determined numerically along with the solutions describing transverse variation of the concentration field. The numerical procedure reduces the governing equations to a system of ten coupled first-order ordinary differential equations, which are integrated in the transverse direction using a standard integration routine.

The results presented here recover the well-known solutions for dispersion in pressure-driven flows when the Debye length is sufficiently large. In this limit, the axial dispersion is proportional to the square of the Peclet number based on the transverse dimension of the tube or channel and is independent of the zeta potential. The skewness in this limit is proportional to the cube of this Peclet number and is also independent of the zeta potential. In the limit

of a small Debye layer thickness, we find that the dispersion varies as the square of the Peclet number based on the Debye length. The skewness varies as the cube of this Peclet number. In this limit, both the dispersion and skewness exhibit a first-order dependence on the zeta potential. Simple approximations to the dependence are presented. We find that increasing values of the zeta potential always reduce both late-time dispersion and skewness.

The methodology devised here for analyzing the late-time transport in electroosmotic flow was also applied to the Taylor problem of pressure-driven flow in a tube and channel. This analysis, presented in Appendix C, yields new analytical solutions describing the axial variation of the mean solute concentration for the problems of an initial planar source and a translating solute interface.

NOMENCLATURE

a	tube radius or channel half-height
c	solute concentration
c_e	ion concentration
D	binary diffusivity
D'	effective diffusivity inclusive of dispersion
E_x	applied axial electric field: $E_x = -d\phi/dx$
f_k	axial concentration functions
F	Faraday constant
g_j	transverse concentration functions
ℓ	distance of travel ($\ell = Ut$)
m	interface ($m=0$) or plane source ($m=1$)
n	channel ($n=0$) or tube ($n=1$)
Pe	Peclet number: $Pe = Ua/D$
R	ideal gas constant
t	time
T	temperature
u	axial fluid speed
$\mathbf{u}$	local fluid velocity
U	mean fluid speed
x	axial position
y	transverse position
z	charge number

α_k	eigenvalues
β	normalized mean fluid speed ($\beta = -\mu U/\epsilon\zeta E_x$)
ϵ	dielectric constant
μ	viscosity
λ	Debye length
ρ_e	charge density
ϕ	electric potential
ζ	surface electric potential

$\mathbf{E}^*$	electric field: $\mathbf{E}^* = -\nabla\phi/E_x$
t^*	time: $t^* = Dt/a^2$
u^*	local fluid speed: $u^* = u/U$
x^*	axial position: $x^* = (x - Ut)/a$
y^*	transverse position: $y^* = y/a$
η	axial position: $\eta = x^*/2\sqrt{t^*}$
λ^*	Debye length: $\lambda^* = \lambda/a$
ζ^*	surface potential: $\zeta^* = zF\zeta/RT$

Subscripts and Superscripts

j, k	order of solution
$*$	asterisk denotes normalized variable
$\bar{}$	bar denotes spatial average
$\hat{}$	hat denotes initial distribution

REFERENCES

1. R. F. Probstein, *Physicochemical Hydrodynamics*, John Wiley & Sons, New York, NY (1995).
2. C. L. Rice and R. Whitehead, "Electrokinetic Flow in a Narrow Cylindrical Capillary," *J. Phys. Chem.*, **69**, 4017, 1965.
3. S. K. Griffiths and R. H. Nilson, "Hydrodynamic Dispersion of a Neutral Non-Reacting Solute in Electroosmotic Flow," SAND99-8249, Sandia National Laboratories, Livermore, CA, 1999. To appear in *Anal. Chem.*.
4. K. H. Haskell, W. H. Vandevender and E. L. Walton, "The SLATEC Mathematical Subprogram Library: SNL Implementation," SAND80-2992, Sandia National Laboratories, Albuquerque, NM, 1980.
5. R. J. Gross and J. F. Osterle, "Membrane Transport Characteristics of Ultrafine Capillaries," *J. Chem. Phys.*, **49**, 228, 1968.
6. S. Levin, J. R. Marriott, G. Neale, G. and N. Epstein, "Theory of Electrokinetic Flow in Fine Cylindrical Capillaries at High Zeta-Potentials" *J. Colloid Interface Sci.*, **52**, 136, 1975.
7. G. I. Tayor, "Dispersion of Soluble Matter in Solvent Flowing Slowly Through a Pipe," *Proc. Roy. Soc. Lond.*, **A 219**, 186, 1953.
8. P. C. Chatwin, "The Approach to Normality of the Concentration Distribution of a Solute in a Solvent Flowing Along a Straight Pipe," *J. Fluid Mech.*, **43**, 321, 1970.
9. R. Aris, "On the Dispersion of a Solute by Diffusion, Convection and Exchange Between Phases," *Proc. Roy. Soc. Lond.*, **A 252**, 538, 1959.
10. H. Poppe, A. Cifuentes and W. T. Kok, "Theoretical Description of the Influence of External Radial Fields on the Electroosmotic Flow in Capillary Electrophoresis," *Anal. Chem.*, **68**, 888, 1996.
11. G. I. Tayor, "Conditions Under Which Dispersion of a Solute in a Stream Can be Used to Mea-

sure Molecular Diffusion," *Proc. Roy. Soc. Lond.*, A **225**, 473, 1954.
12. R. Aris, "On the Dispersion of a Solute in Fluid Flowing Through a Tube," *Proc. Roy. Soc. Lond.*, A **235**, 67, 1956.
13. R. A. Wooding, "Instability of a Viscous Liquid of Variable Density in a Vertical Hele-Shaw Cell," *J. Fluid Mech.*, **7**, 501, 1960.

ACKNOWLEDGMENT

The authors wish to thank Dr. R. S. Larson for his very careful review of this paper. This work was funded by a Sandia Phenomenological Modeling and Engineering Simulations LDRD. Sandia National Laboratories is operated by Sandia Corporation for the United States Department of Energy.

APPENDIX A: INITIAL AND BOUNDARY CONDITIONS

In the present study we consider two fundamental problems. The first is the transport in the vicinity of a traveling solute interface, as indicated by $m=0$. The second is the transport of a solute peak following injection of a instantaneous planar source into the fluid stream. This problem is indicated by $m=1$.

The initial conditions for these two problems are described by $c^*(x^*,y^*,t^*) = \hat{c}^*(x^*)$ at $t^* = 0$, where

$$\hat{c}^* = \frac{1}{2}\operatorname{erfc}\frac{x^*}{2\sqrt{t^*}} \quad \text{as} \quad t^* \to 0 \qquad \text{(A1)}$$

for the interface, and

$$\hat{c}^* = \frac{e^{-x^{*2}/4t^*}}{2\sqrt{\pi\, t^*}} \quad \text{as} \quad t^* \to 0 \qquad \text{(A2)}$$

for the planar source. The first of these approximates an initial unit step at $x^*=0$, while the second approximates an initial plane source of unit strength centered at $x^*=0$. Since we are interested here in a late-time solution, it is convenient to express the initial conditions in terms of moments of the solute distribution. That is,

$$\int_{-\infty}^{\infty} x^{*p} \int_0^1 (c^* - \hat{c}^*)\, y^{*n} dy^* dx^* = 0 \qquad \text{(A3)}$$

as $t^* \to 0$, for all $p \geq 0$. If all moments of the functions $c^*(x^*,y^*,t^* \to 0)$ and $\hat{c}^*(x^*)$ exist and are equal, then the two functions are the same.

In terms of the normalized variables, the initial conditions (A2) and (A3) require that

$$\int_{-\infty}^{\infty} 2f_0\, d\eta = 1 \qquad m = 1 \qquad \text{(A4)}$$

for the case of the planar source. The initial condition (A3) additionally requires that the higher-order functions f_k for both the translating interface, $m=0$ and instantaneous plane source, $m=1$, must also satisfy

$$\int_{-\infty}^{\infty} \eta^p f_k\, d\eta = 0 \quad \text{for} \quad 0 \leq p \leq k+m-1 \qquad \text{(A5)}$$

for all $k \geq 1$. Higher-order moments of f_k need not vanish since the net exponent of the time in the corresponding terms of Eq. (A3) is greater than zero for $p > k+m-1$.

Boundary conditions for the normalized concentration are $c^* \to 1$ as $x^* \to -\infty$ and $c^* \to 0$ as $x^* \to \infty$ for the case of a translating interface, and $c^* \to 0$ as $x^* \to \pm\infty$ for the instantaneous plane source. In terms of the normalized variables, the corresponding boundary conditions for the functions f_k are $f_0 \to 1$ as $\eta \to -\infty$ and $f_0 \to 0$ as $\eta \to \infty$ in the case of a translating interface, and $f_0 \to 0$ as $\eta \to \pm\infty$ for the instantaneous planar source. Boundary conditions for higher-order functions in both cases are $f_k \to 0$ as $\eta \to \pm\infty$.

APPENDIX B: RANGE OF APPLICABILITY

The series solution given by Eq. (15) applies rigorously only in the limit $t^* \to \infty$. Nevertheless, such a series may provide quite accurate estimates of the concentration field for finite values of t^*, provided that these values are sufficiently large. Here we address this applicable range of t^* for that part of the series describing the mean axial variation of the concentration field.

Because we have obtained solutions for both the zeroth and first-order terms, the accuracy and applicable range of the zeroth-order solution can be obtained by comparing its magnitude with that of the first-order correction. From the form of Eq. (15), the condition for applicability may thus be written

$$\frac{|f_1|}{2\sqrt{t^*}|f_0|} \ll 1 \qquad \text{(B1)}$$

This expression yields criteria that differ slightly for the tube and channel geometries, as well as for the

interface and plane source problems. By neglecting constants of order unity, however, we can obtain from Eq. (B1) a conservative estimate of the condition for applicability of the series. The result is

$$t^* = \frac{Dt}{a^2} = \frac{\ell}{aPe} \gg \frac{\alpha_1^2 Pe^6}{\left(1+\alpha_0 Pe^2\right)^3} \qquad \text{(B2)}$$

where $\ell = Ut$ is the distance of travel over a fixed time, t, at the fixed mean speed, U. The neglected constants for the various special cases would all appear in the denominator of Eq. (B2), and all of these are greater than one over the range of η where the solutions are non-trivial.

Equation (B2) exhibits two useful limiting behaviors. The first of these holds for $\alpha_0 Pe^2 \ll 1$. In this diffusion-dominated limit, the condition for applicability becomes

$$t^* \gg \alpha_1^2 Pe^6 \qquad \text{(B3)}$$

The second limiting behavior holds for $\alpha_0 Pe^2 \gg 1$ or equivalently $Pe \gg \sqrt{1/\alpha_0}$. Note that this is a generalization of the condition that Taylor gave for neglecting diffusion in pressure-driven flows [11]. In this convection-dominated limit, the condition (B2) becomes

$$t^* \gg \frac{\alpha_1^2}{\alpha_0^3} \quad \text{or} \quad \frac{\ell}{a} \gg \frac{\alpha_1^2 Pe}{\alpha_0^3} \qquad \text{(B4)}$$

The right-hand form of this expression is again functionally equivalent to that given by Taylor for pressure-driven flow in a tube, though the form above remains valid for all profiles of the fluid velocity and for both tube and channel geometries.

In the special case in which λ^* is small and convective transport is dominant, the condition for applicability given by Eq. (B4) becomes independent of λ^*. It instead depends only on the normalized zeta potential. This is apparent from the forms of Eqs. (B4), (49) and (51) for a tube or Eqs. (B4), (54) and (55) for a channel. For a tube, this limiting behavior of Eq. (B4) is

$$t^* \gg \frac{1}{18}\frac{h_1^2}{h_0^3} \quad \text{as} \quad \lambda^* \to 0 \qquad \text{(B5)}$$

where h_0 and h_1 are given by Eqs. (50) and (52). The comparable result for a channel is

$$t^* \gg \frac{128}{2025}\frac{h_1^2}{h_0^3} \quad \text{as} \quad \lambda^* \to 0 \qquad \text{(B6)}$$

The functions h_0 and h_1 for a channel are the same as those for a tube, as discussed earlier in the text.

APPENDIX C: THE TAYLOR PROBLEM

In 1953 and 1954, Sir Geoffrey Taylor wrote two important papers concerning the origins and analysis of hydrodynamic dispersion [7,11]. This phenomenon, resulting from the nonuniform profile of the fluid speed across a tube or channel, yields an axial variation of the late-time solute distribution identical to that resulting from a diffusion process alone. Remarkably, the only distinction is that the apparent diffusivity of the dispersion process is not a constant, but instead varies as the square of the Peclet number.

Taylor's first paper [7] laid out the essential features of dispersion in pressure-driven flow in a tube and provided an analytical solution for the late-time transverse variation of the solute concentration in terms of the local gradient of the mean axial variation. This analysis was based largely on an insight that some additional flux, beyond that due to diffusion, crossed the origin of a coordinate system that translated with the mean speed of the flow. The extra flux, he concluded, was proportional to the solute concentration gradient and therefore must be due to dispersion mimicking the behavior of ordinary diffusion. Taylor reached this conclusion by means of his considerable intellect and provided the reader little detailed justification.

In his second paper [11], Taylor presented a more rigorous derivation of his original result. Here, as in the original paper, he neglected the contribution of axial diffusion, but extended the solution to include first-order and second-order corrections to the transverse variation of the solute concentration. Again these results were expressed in terms of spatial derivatives of the mean axial concentration profile, so neither of Taylor's first two papers directly address this axial variation of the solute concentration.

Aris [9,12] later generalized Taylor's analysis to include arbitrary tube cross-sections and extended the solution by including the contribution of axial diffusion and chemical reactions with a stationary phase. Expanding the solution in terms of spatial moments of the solute concentration, Aris reproduced Taylor's results and further provided a rigorous basis for treating a variety of initial conditions. Nevertheless, his use of moments again relegated the true axial variation of the solute concentration to a somewhat secondary concern.

More recently, Chatwin [8] employed a late-time series to analyze the approach to a normal distribution of the mean axial solute concentration for very general initial conditions. His paper clearly

states the limitations of the previous analyses discussed above. The present analysis closely resembles that of Chatwin in that both employ a series expansion in inverse powers of the square-root of time and both yield the full axial and transverse variation of the concentration field. Chatwin's solutions, however, are presented in terms of Hermite polynomials for generalized initial conditions, making evaluation of his results for the simple problems of an initial planar source or traveling interface a bit difficult. Moreover, he provided explicit expressions for the coefficients describing transport in a tube only for the case of infinite Peclet number and only for the problem of a instantaneous planar source. Even in this case, Chatwin provided no simple expressions equivalent to Eqs. (43) through (47). As a result, direct comparison of Chatwin's solutions with the present results is sufficiently complex that we have not been able to confirm with certainty that the two results are identical. We believe that this is the case, however, owing to the fact that certain rational numbers appear in both. Further, the transverse variation of the late-time concentration field is clearly the same in both and the same as that obtained by Taylor [11].

Since 1953 the Taylor and Aris papers have been referenced several thousand times. In 1998-99, Taylor's first papers alone have received over 150 citations. Despite this continued and widespread interest in dispersion, Chatwin's paper in 1970 appears to be the only published account of the first-order late-time correction to the axial solute distribution. Here we apply the present methodology to this classic problem.

Equations (43) and (44) above are the zeroth-order and first-order terms describing the late-time transport of a traveling interface near the leading edge of a semi-infinite non-reacting solute band. Equations (46) and (47) similarly describe the late-time transport of an initial planar source. These expressions are valid for all velocity profiles and applicable to both the tube and channel geometries. The influence of the velocity and geometry appears only through the eigenvalues, α_0 and α_1, determined by Eqs. (23) and (24). Likewise, the equations governing the transverse variation of the concentration field are given by Eqs. (18) and (19) for all velocity profiles and for both tube and channel geometries.

For the case of laminar flow in a tube, the fluid velocity is given by the well-known parabolic relation

$$u^* = 2\left(1 - y^{*2}\right) \qquad \text{(C1)}$$

From Eqs. (18) and (19) and the prescribed boundary conditions, this velocity profile yields

$$g_1 = -\frac{1}{24}\left(2 - 6y^{*2} + 3y^{*4}\right) \qquad \text{(C2)}$$

and

$$g_2 = \frac{1}{11520}\left(31 - 180y^{*2} + 300y^{*4} - 200y^{*6} + 45y^{*8}\right) \qquad \text{(C3)}$$

These two expressions describing the transverse variation of the concentration field are exactly the same as those obtained by Taylor and by both Chatwin and Aris for this problem. Equations (22) and (23) similarly yield

$$a_0 = \frac{1}{48} \quad \text{and} \quad a_1 = -\frac{1}{2880} \qquad \text{(C4)}$$

The first of these is Taylor's famous result. The second appears to be the result obtained by Chatwin for the case of an infinite Peclet number. Aris [9] gave an expression for the late-time skewness of the concentration profile, in principle related to α_1, but a direct analogy with his result cannot be drawn.

The results obtained here clearly parallel those of previous studies. However, earlier results, with the exception of Chatwin's solution, were obtained in the absence of any explicit description of the axial variation of the mean solute concentration. Expressions paralleling Eq. (15) and Eqs. (43) through (47) in this study were not provided. Moreover, even Chatwin's very general solution does not readily yield these expressions. Thus, while the results above are familiar, they represent an extension of previous work in the context of Eqs. (15) and (43) through (47).

The applicable range of these results for use in Eqs. (43) through (47) is given in Appendix B. In the diffusion-dominated limit, Eq. (B3) yields the condition $t^* \gg Pe^6/8294400$ for the valid range of f_0. The result from Eq. (B4) in the convection-dominated limit is $\ell/a \gg Pe/75$. As noted just before Eq. (B4), the requirement for such convection-dominated behavior is $Pe \gg \sqrt{1/\alpha_0} \approx 6.9$. This is exactly the requirement stated by Taylor [11]. However, the preceding condition is more lenient than Taylor's, which he stated as $\ell/a \gg Pe/4$.

The profile of the fluid velocity in a channel of infinite width is also well known and is given by

$$u^* = \frac{3}{2}\left(1 - y^{*2}\right) \qquad \text{(C5)}$$

For this case, the transverse variation of the concentration field is described by

$$g_1 = -\frac{1}{120}\left(7 - 30\,y^{*2} + 15\,y^{*4}\right) \qquad \text{(C6)}$$

and

$$g_2 = -\frac{1}{201600}\left(29 + 1020\,y^{*2} - 3570\,y^{*4} + 2940\,y^{*6} - 675\,y^{*8}\right) \qquad \text{(C7)}$$

We find no published account of these solutions. The corresponding eigenvalues for the case of a channel are

$$a_0 = \frac{2}{105} \quad \text{and} \quad a_1 = \frac{4}{1735} \qquad \text{(C8)}$$

The first of these was published by Aris [9] in 1959 and popularized by Wooding [13] in 1960. The Aris result was obtained by moment methods without solving explicitly for the axial variation of the concentration field. The second result does not seem to have been published.

The applicable range of these results is again given by Eqs. (B3) and (B4). In the diffusion-dominated limit, the condition for applicability becomes $t^* \gg 16Pe^6/3010225$. The condition for the convection-dominated limit becomes $Pe \gg \sqrt{105/2} \approx 8.7$, about the same as that for a tube. The corresponding condition for validity of the zeroth-order solution is, however, much more stringent. For convection-dominated transport in a channel, this is given by $\ell/a \gg 92610\,Pe/120409 \approx Pe/1.30$.

All of the solutions presented above were confirmed by direct finite-difference numerical simulation of the transient transport problem. The axial distribution of the concentration field given in Eqs. (42) through (46) was similarly confirmed for both tube and channel geometries.

UNLIMITED RELEASE
INITIAL DISTRIBUTION

K. F. Jensen
Massachusetts Institute of Technology
Building 6-469
Chemical Engineering
Cambridge, MA 02139

1413 T. E. Michalske, 1115
1425 D. R. Adkins, 1715
1425 G. C. Frye-Mason, 1715
0710 A. P. Sylwester, 6245
0149 C. E. Meyers, 4000
1094 M. C. OBorny, 7524
9001 M. E. John, 8000
Attn: D. R. Henson, 8400
9056 J. Vitko, 8100
9056 D. L. Lindner, 8102
9671 J. S. Schoeniger, 8120
9214 C. F. Melius, 8130
9054 W. J. McLean, 8300
Attn: D. R. Hardesty, 8361
F. P. Tully, 8353
R. W. Carling, 8362
9671 E. B. Cummings, 8355
9401 J. M. Hruby, 8355
9051 P. H. Paul, 8355
9056 L. A. Rahn, 8351
9671 D. W. Arnold, 8358
9671 C. G. Bailey, 8358
9161 W. Bauer, 8358
9671 D. J. Rakestraw, 8358
9405 T. M. Dyer, 8700
Attn: R. Q. Hwang, 8721
K. L. Wilson, 8722
J. C. F. Wang, 8723
G. J. Thomas, 8724
W. A. Kawahara, 8725
E. P. Chen, 8726
J. L. Handrock, 8727
9042 S. K. Griffiths, 8728 (5)
9051 R. S. Larson, 8728
9042 R. H. Nilson, 8728 (5)
9042 M. W. Perra, 8728
9214 R. C. Armstrong, 8980
0841 P. J. Hommert, 9100
0826 W. L. Hermina, 9111
0826 D. R. Noble, 9111
0826 P. R. Schunk, 9111
0843 A. C. Ratzel, 9112
0827 C. C. Wong, 9114
1003 B. L. Spletzer, 9611

9018 Central Technical Files, 8940-2 (3)
0899 Technical Library, 4916
9021 Technical Communications Dept., 8815/
Technical Library, MS 0899, 4916
9021 Technical Communications Dept., 8815
for DOE/OSTI

This page intentionally left blank